OMAE 2012-83388

EXPERIMENTAL INVESTIGATION OF IRREGULAR WAVE CANCELLATION USING A CYCLOIDAL WAVE ENERGY CONVERTER

Stefan G. Siegel[*]

Department of Aeronautics
United States Air Force Academy
Air Force Academy, Colorado, 80840
USA
Email: stefan@siegels.us

Casey Fagley

Department of Aeronautics
United States Air Force Academy
Air Force Academy, Colorado, 80840,
USA

Marcus Römer

Department of Aeronautics
United States Air Force Academy
Air Force Academy, Colorado, 80840,
USA

Thomas McLaughlin

Department of Aeronautics
United States Air Force Academy
Air Force Academy, Colorado, 80840,
USA

ABSTRACT

The ability of a Cycloidal Wave Energy Converter (CycWEC) to cancel irregular deep ocean waves is investigated in a 1:300 scale wave tunnel experiment. A CycWEC consists of one or more hydrofoils attached equidistant to a shaft that is aligned parallel to the incoming waves. The entire device is fully submerged in operation. Wave cancellation requires synchronization of the rotation of the CycWEC with the incoming waves, as well as adjustment of the pitch angle of the blades in proportion to the wave height. The performance of a state estimator and controller that achieve this objective were investigated, using the signal from a resistive wave gage located up–wave of the CycWEC as input. The CycWEC model used for the present investigations features two blades that are adjustable in pitch in real time. The performance of the CycWEC for both a superposition of two harmonic waves, as well as irregular waves following a Bretschneider spectrum is shown. Wave cancellation efficien-cies as determined by wave measurements of about 80% for the majority of the cases are achieved, with wave periods varying from 0.4s to 0.75s and significant wave heights of $H_s \approx 20mm$. This demonstrates that the CycWEC can efficiently interact with irregular waves, which is in good agreement with earlier results obtained from numerical simulations.

NOMENCLATURE

T   Wave Period [s]
D   Water Depth [m]
H_s Significant Wave Height [m]
W   Wave, index indicates type of wave
C   Wave Travel Velocity (Celerity) [m/s]
C_g Wave Group Velocity [m/s]
C_r Beach Reflection Coefficient $C_r = \frac{H_{reflected}}{H_{incoming}}$
ρ Fluid Density [kg/m^3]
k   Wave Number [1/m]

---

[*]Address all correspondence to this author.

g   Gravity constant, $9.81[m/s^2]$
t   Time [s]
λ   Wavelength [m]
$R = 60mm$ Wave Energy Converter Radius [m]
$c = 50mm$ Hydrofoil Chord [m]
$s = 550mm$ Hydrofoil Span [m]
x_c, y_c Wave Energy Converter Shaft location [m]
η   Water Surface [m]
α   Hydrofoil pitch angle relative to tangential direction [○]
γ   Flap wave maker angle [°]
T_F Wave maker period [s]
$δ(t)$ Main Shaft rotational angle [°]
θ   Phase [°] between wave maker and WEC main shaft

1   Introduction

Among alternative energy sources, wave power is one of the most abundant sources on earth. The World Energy Council according to [1] has estimated the world wide annual amount of wave power energy at 17.5 PWh (Peta Watt hours = $10^{12}kWh$). This amount of power is actually comparable to the annual world wide electric energy consumption, which is currently estimated at 16 PWh. Thus, wave power has the potential to provide a large portion of the worlds electric energy needs, if it can be harnessed efficiently. In addition to the energy availability, wave power has other advantages. Since a large portion of the worlds population lives close to the ocean shores, the distance between energy production and consumption is small, which reduces transmission losses and necessary investments in transmission lines. As opposed to other alternative energy sources like wind, stream and solar energy, the installation of wave power devices does not require use of already precious real estate. This makes wave power an ideal energy source for efficiently providing renewable energy to densely populated coastal areas. Ocean waves have a tremendous potential to provide clean renewable energy. Further engineering aspects of wave power as an energy source are appealing as well. While the power density of both solar and wind in typical favorable sites is in the order of $1\,kWm^{-2}$ [2], wave power in a typical North Atlantic wave that was considered in a related paper [3] (wave height of $H = 3.5m$ and period of $T = 9s$) yields $108\,kWm^{-1}$ of wave crest. As shown there, a device extending about $40m$ in the vertical direction can extract almost all of this wave power, yielding a power density of about $2.7kWm^{-2}$ or more than two and a half times that of wind or solar power. If one considers the theoretical inviscid conversion limits for waves and wind, which are 100% for waves [4] and 59% for wind [5], the accessible power density of waves is more than four times as large as that of wind. Furthermore, wave energy is available on a more consistent basis and can be better predicted in advance, therefore mitigating the need to back up a wave power plant with other conventional power sources, such as solar and wind energy.

2   Motivation and Objectives

Analysis of the different wave energy conversion devices that have been investigated or proposed reveals a number of commonalities in design. The first is that all devices require a connection to the sea bed in order to extract energy, which has two main drawbacks. First, a seabed connection makes the device vulnerable in rough seas and storms, in the same way as an anchored ship is vulnerable in a storm (and will likely break the anchor line). According to [1], storm survivability has been a major problem for many wave energy converters, with some being destroyed by the elements as early as during deployment. Also, for most of the devices, the load imposed onto the seabed connection is proportional to the power which the device can extract. This means that the anchor point needs to be stronger and thus more costly as more energy is being extracted. Therefore, many of these devices cannot easily be scaled up to industrial power plant levels of energy conversion. In addition, since the devices need to be anchored to the sea floor, they are not well suited to operation in deep water waves, where the ocean floor may be hundreds of meters away from the surface. However, most wave energy is contained in deep water waves, and the energy density of a wave decreases as it approaches shallow water. Thus, most devices cannot operate in the most promising locations for wave power extraction.

Beyond survivability, efficiency has been a major issue for many WEC designs. While wave energy as a resource may be free, the construction effort to harness it is a major expense and to a large degree determines the cost of energy being produced. As a less efficient WEC will need to be larger in size to extract the same amount of energy as a more efficient one, cost of energy is directly related to efficiency. Arguably, the most efficient WEC is one that can extract all of the energy from an incoming wave, and the class of wave energy converters that is able to achieve this is commonly referred to in literature as wave termination devices. There have been various wave termination designs reported in literature, with the most well known devices being the Salter Duck [6] and the Bristol or Evans Cylinder [7]. Both consist of a series of elements which are aligned parallel to the wave crests, in the case of the Salter Duck these are cam–shaped and floating on the surface, while the Bristol Cylinder is fully submerged. Both have been shown to be able to absorb an incoming wave completely. The wave energy is converted to electric power by means of a power–take–off system that is hydraulic in both cases. As both devices move at approximately the wave induced water velocity, the devices need to feature a large surface area to convert appreciable amounts of power. This increases construction cost, reduces storm survival odds and has ultimately motivated the investigation of the Cycloidal WEC described here. The fact that both devices require mooring to the ocean floor also hampers storm survival odds and precludes installation in very deep water.

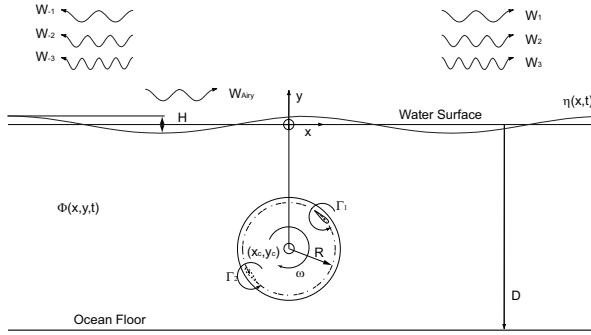A typical cycloidal wave energy converter (CycWEC) as

Figure 1. Cycloidal wave energy converter geometry and generated waves

considered in this paper is shown in figure 1. It features one or more hydrofoils attached eccentrically to a main shaft at a radius R. While the shaft rotates, the pitch angle of the blades may be adjusted. This device operates at a rotational speed of the hydrofoil that is typically an order of magnitude larger than the wave induced water velocity, and employs the lift force at the hydrofoil to generate shaft torque directly. Using lift allows for a much smaller hydrofoil plan form area to be employed compared to the cross sectional areas of Duck and Cylinder, and generating shaft torque directly eliminates the need for a costly and inefficient hydraulic power take off system. In addition, it is conceptually possible to join several CycWECs into a cluster where the reactive forces at the shaft can be made to cancel, which reduces or negates entirely the need for mooring and thus enables deep water deployment while improving storm survival odds (see Siegel [8] for sketches). The fact that the reactive force changes direction though 360° with each wave passage enables force cancellation if the individual WECs are spaced half a wavelength apart, thus causing reactive forces of same magnitude but opposite direction.

A single rotating hydrofoil was first investigated by Hermans et al. [9] both numerically and experimentally. While Hermans et al. reported very low wave energy conversion efficiencies (on the order of a few percent), Siegel et al. [3] were able to show in simulations that with improved sizing of the WEC as well as by using synchronization of the rotation of the foil with the incoming wave, wave termination with better than 99% inviscid efficiency was possible. These numerical findings were confirmed by 1:300 scale experiments in 2011, as reported by Siegel et al. [10] where invisicid conversion efficiencies of greater than 95% were achieved in the same facility employed in this study. Both of these initial studies performed synchronization of the WEC with a numerically generated harmonic wave, or a paddle wave maker, respectively. Thus they did not require a feedback controller and estimator to succeed. A controller and estimator were for the first time successfully implemented by Jeans et al. [11] for irregular waves in a numerical simulation. Typical

conversion efficiencies in this study were beyond 90% for a superposition of two harmonic waves, and around 80% for irregular waves following a Bretschneider distribution. At the same time, the controller and estimator were successfully tested in an experiment as reported in [12] where harmonic waves with different wave heights and frequencies were successfully cancelled, achieving efficiencies comparable to the earlier synchronization experiments that had a priori knowledge of the incoming wave. The performance of the feedback controller and estimator could thus be experimentally verified for the first time.

In the present study, the CycWEC investigations are advanced by experimentally canceling both a superposition of two harmonic waves, as well as irregular waves following a Bretschneider distribution. While this has been done in simulations reported by Jeans et al. [11], so far no experimental validation for these types of waves interacting with a CycWEC exists. By first investigating the interaction of the CycWEC with two harmonic waves, the performance of the pitch control mechanism is established first, since the resulting wave pattern exhibits a strong amplitude modulation with the frequency difference of both waves. An incoming wave field following a Bretschneider distribution then adds variations in frequency to the wave field in a way that is typically encountered in deep ocean waves. The performance of the CycWEC in cancelling this wave field can thus be considered representative for the performance of the device in a deep ocean setting at full scale.

3 Experimental Setup

The tunnel used for testing the cycloidal WEC was a 2D wave tunnel designed to provide a 1:300 scale model of a deep ocean wave. The full scale design deep ocean wave, which was investigated numerically in [3] had a period of 9s, a wave length of 126.5m and a wave height of 3.5m, and it carried about 105kW of power per meter of wave crest. It was represented in the present setup by a wave with a period of 0.5s and wave length of 0.39m; at a typical wave height of 20mm the scaled wave carried approximately 192mW of wave power per meter. The experiment consisted of four subparts: Wave tunnel, CycWEC model, wave gages and Data Acquisition (DAQ) and processing system. In addition, a feedback controller and state estimator were employed to operate the CycWEC. All of these components are described in detail in the following subsections.

3.1 Wave Tunnel

The wave tunnel is shown as conceptual sketch in figure 3. It allowed for the generation of waves with a period between 0.2 and 1.15 seconds, and consisted of the following three parts:

3.1.1 The wave tank The tank had an overall length of 5m, where 4.50 meter were usable for wave experiments between

the flap wave maker and the beach, a width of 0.55m and a design water depth of 0.3m. The width of the tunnel was increased by 50mm on each side in the center test section, which allowed the drive system of the CycWEC to be placed outside of the wave testing area by means of false walls. The Eigenfrequency of the wave tunnel, which corresponds to a standing wave spanning the length of the tunnel with an integer multiple of wave lengths, had a period of 5.5-6 seconds, which was determined by exciting the tunnel resonance using a step input at the wave maker.

3.1.2 The beach

The beach, located at the right end of the tunnel, was a linear beach with a 1:4 slope. The main purpose was to prevent reflection of waves travelling left to right. In order to evaluate the wave reflections from the beach, the reflection coefficient was measured experimentally and also compared to predictions based on a well established numerical model. At the design wave of $T = 0.5s, H = 20mm$ the reflection coefficient was measured by traversing two wave gages using the approach described in [7] and found to be $C_r = 0.106$. This was less than the estimate from the numerical model described in [13], which for the design wave estimated the reflection coefficient to be $C_r = 0.17$ which is the ratio between reflected and incident wave. We thus considered the numerical model a worst case estimate, and given textbook statements that consider it difficult to achieve less than $C_r = 0.1$ [14] the beach was found to perform sufficiently well for the measurements at hand. No wave reflection prevention (e.g. wave cancelling wave maker) was available at the left end of the tunnel for waves travelling right to left, where the flap wave maker was located. This did not cause any significant impact on the results, though, since the wave heights on the up–wave side of the WEC model were minimal for all data presented.

3.1.3 Irregular Wave Synthesis

The irregular incident wave field is created using a linear superposition of a finite number of linear Airy wave components. The resulting surface elevation for a unidirectional deep ocean wave propagating in the x-direction and satisfying the linearized free surface boundary conditions is given in [15] to be,

$$\eta_I(x,t) = \sum_{i=1}^{N_I} \frac{H_i}{2} cos\left(k_i x - \omega_i t + \theta_i\right), \qquad (1)$$

where N_I is the number of regular wave components used to represent the irregular wave field, and H_i, k_i, ω_i and θ_i are the wave height, number, frequency and phase for component i, respectively. The wave phase components θ_i are obtained using a random number generator based on a uniform distribution between 0 and 2π. The fidelity of the irregular wave field will increase as

the number of wave components is increased. According to [16], a minimum of 20 wave components are required for modelling a unidirectional irregular seaway.

The amplitude for component i is based on a specified wave spectrum according to,

$$a_i = \frac{H_i}{2} = \sqrt{2S_I(\omega_i)\Delta\omega_i}, \qquad (2)$$

where S_I is the spectral density and $\Delta\omega_i$ is the wave frequency interval for component i.

For the current study the the incident wave field is modelled using the Bretschneider wave spectrum, which is a commonly used two parameter model for wave spectra in the open ocean. The 15th International Towing Tank Conference [17] defines the Bretschneider spectrum as,

$$S_I(\omega) = \frac{486.0H_s^2}{T_p^4\omega^5} \exp\frac{-1948.2}{T_p^4\omega^4}, \qquad (3)$$

where H_s is the significant wave height and T_p is the wave period associated with the peak energy. The Bretschneider wave spectrum for $H_s = 3.25$ m and $T_p = 9.7$ s (i.e. sea-state 5) is shown in Fig. 2(a). Also shown are the resulting wave components when the spectrum is divided into 21 wave components with $\omega_{min} = 0.4$ rad/s, $\omega_{max} = 2.0$ rad/s, and $\Delta\omega_i = 0.08$ rad/s. Each wave component is identified numerically in Fig. 2(a) and is referred to as $W_{I1} - W_{I21}$ throughout the remainder of the paper. The amplitude of each wave is determined from Equation 2.

With the period and amplitude of each component wave defined, the associated wave length and power can be determined from Airy wave theory. The wave length is determined from the dispersion relationship,

$$\lambda_i = \frac{T_i^2 g}{2\pi}, \qquad (4)$$

where λ_i and T_i are the wavelength and period of component i. The wave power per unit length, P_i, associated with each component is related to the wave height and period,

$$P_i = \frac{1}{32\pi}\rho g^2 H_i^2 T_i, \qquad (5)$$

where ρ is the density of water (assumed to be $\rho = 1000$ kg/m^3 for this study). Since the wave power scales linearly with the wave period, higher harmonic waves of the same wave height will contain less energy in proportion to their period. Also note the quadratic relationship between wave energy and wave height.

4
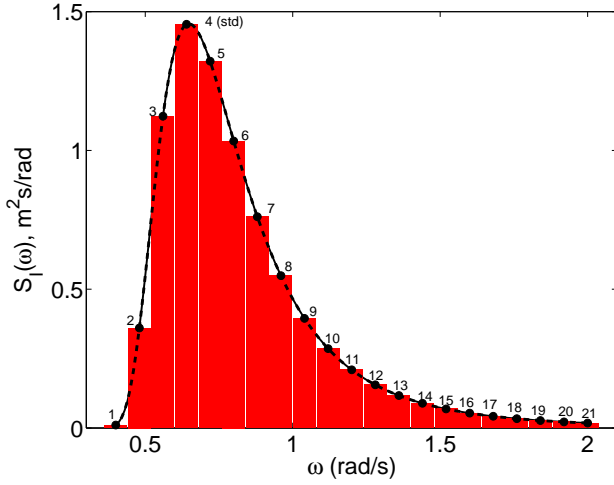
(a) Bretschneider energy spectrum for $H_s = 3.25$ m and $T_p = 9.7$ s (i.e. sea-state 5).
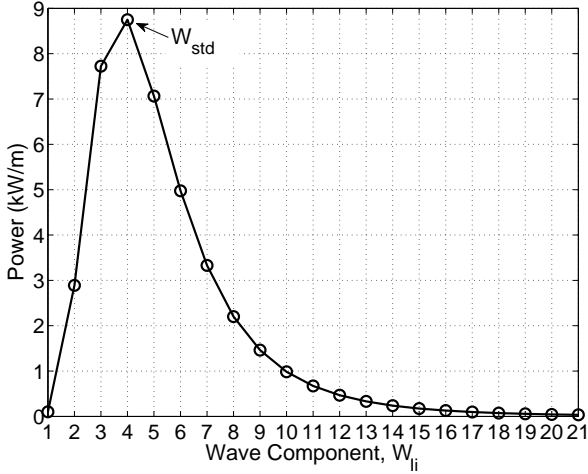
(b) Associated power of each of the 21 discrete wave components.

Figure 2. Incident wave field modelled using the Bretschneider wave spectrum and 21 discrete wave components based on Airy wave theory.

For the full scale ocean wave, the power associated with each component wave in Fig. 2(a) is shown in Fig. 2(b). The total power of all 21 components is 41.79 kW/m and W_{I4} has the peak power of all individual components with 8.75 kW/m.

The wave spectra with different amounts of component waves were scaled from full scale to tunnel scale, where the wave period for the most dominant component I_4 was $T_4 = 0.5s$. The corresponding significant wave height was $H_s = 15mm$.

3.1.4 The flap wave maker The flap wave maker was a plain flap hinged at the bottom of the tunnel. It was driven by a
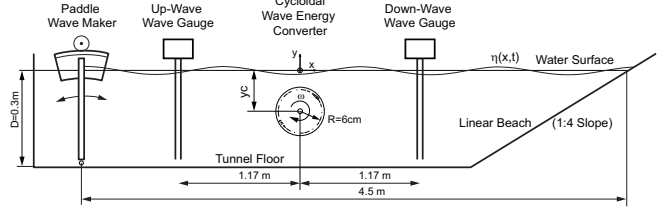

Figure 3. Wave tunnel schematic - not to scale

brush type servo motor driving two sprockets attached to a shaft spanning the tunnel, which engaged in two arc gear segments located at both sides of the tunnel attached to the top of the flap. This setup provided gearing to match the torque characteristics of the servo motor to the torque requirements of the wave maker. It also ensured pure rotational motion of the flap without torsion. The servo motor was connected to a motion controller operating in position mode allowing for arbitrary motion wave forms with an update rate of 10ms. In the present investigations, either a Bretschneider spectrum superposition of harmonic waves as described in the previous section, or a double sinusoidal motion

$$\gamma(t) = \delta_1 \sin(2\pi t / T_1) + \delta_2 \sin(2\pi t / T_2) \qquad (6)$$

was prescribed using a deterministic hardware timed LabVIEW loop. This setup had the advantage that both wave height and period could be computer controlled without any hardware adjustments. It did not provide any incoming wave cancellation since no force feedback was available. Given the resolution of 2000 pulses per revolution of the servo motor shaft mounted encoder, and the gear ratio of 10:1 an angular resolution of 0.018 degrees was achieved.

Figure 3 shows a sketch of the overall test setup. The flap wave maker generated waves at the left side of the tunnel, which traveled past the first wave gage (up–wave wave gage). In the center of the test section the wave reached the CycWEC. The remaining waves were measured by the second wave gage, which was located at an equal distance from the CycWEC. After a short distance the waves dissipated their energy at the beach.

3.2 Wave Energy Converter Model

Based on the sketch in figure 1, a number of non–dimensional quantities emerged. The basic size of the wave energy converter was denoted by $2R/\lambda$, where the wave length λ was the fundamental length scale. Consequently, the vertical position of the main shaft was denoted by y_c, and the wave height by H. It was also convenient for parameter studies to compare different size wave energy converters while keeping the distance between the water surface and the topmost point of the cycloidal wave energy converter path fixed, that is $|y_c| - R = const$. The direction of travel of an incoming ocean wave W_{Airy} was assumed

to be left to right. Waves generated by the cycloidal wave energy converter that travelled in the direction of the incoming wave received a positive index and were considered travelling down–wave; while waves in the opposite direction were considered up–wave travelling and received a negative index number.

The CycWEC device was designed to convert energy from waves to shaft power by wave cancellation. Figure 4 shows a CAD model, while the definition of the main geometry parameters is shown in figure 1. The only component interaction with the flow were two hydrofoils spanning the tunnel. These hydrofoils were attached eccentrically at a radius $R = 60mm$, and had a NACA 4 series hydrofoil of $c = 50mm$ chord length, with a camber line curvature to match the radius of the circle on which it rotated. The hydrofoil had a resulting camber line displacement of 11 percent, and the maximum thickness of 15% was located at 50% chord. This setup provided a zero–lift pitch angle of approximately $0°$ and was expected to behave like the familiar NACA 0015 in straight flow, when rotating around a shaft.

The CycWEC was installed in the center of the wave tunnel such that the waves travelling the length of the tunnel were unobstructed but for the interaction with the CycWEC blades. The CycWEC could be operated with one or two blades, however all results presented in this paper were obtained with two blades. The main shaft motor was located outside the water well above the tunnel, and connected directly to two timing belt sprockets. The timing belts engaged in individual larger sprockets below the water line with a 5:1 gear ratio, which in turn held the blades. The main shaft motor (Pittman model 4442 S012) was a brushless servo motor with a 500 lines/rev incremental encoder driving the main shaft directly, and connected to a closed loop servo motor controller (Copley Motion Accelnet ACJ-090-12) allowing the motor to operate both as motor or generator depending on the torque applied to the shaft. Together with the 5:1 gear ratio as well as edge detection of the encoder signals, an overall resolution of 10000 counts/revolution was achieved. The motor controller was operated in position mode, with position updates transmitted every 10ms to the controller over the CAN bus system (see below).

The pitch angle of each blade was adjustable under computer control in real time. This was achieved by means of two digital model aircraft servos, which were attached to the main shaft located outside the water. The servos turned a second timing belt sprocket by means of a gear attached to the servo shaft. The sprocket then adjusted the pitch of the blade by means of a second set of timing belts and 5:1 larger sprocket arranged concentrically with the drive sprocket, which connected to a push rod that was attached to the blade. The servos had a range of motion of $\pm 60°$, and with an overall gear ratio of 3:1 the blades could be adjusted over a range of approximately $\pm 20°$. The transmission also improved the positioning accuracy of the servos, which was measured to be $\pm 0.5°$, to one third of that, or $\pm 0.17°$.

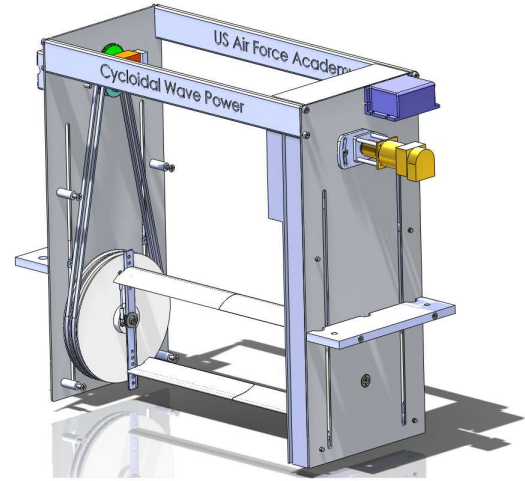The sign convention for the pitch angle was chosen such that

Figure 4. Picture of wave energy converter with a two blades and pitch control.

a rotation of the blade's leading edge towards the rotation center was negative, a rotation outward positive. For the present investigation, the blades were pitched in opposite direction at all times, which was found to provide the best performance in previous numerical studies. The pitch angle magnitude was kept equal for both foils.

The depth to which the rotational center of the WEC was submerged below the mean water surface, y_c, could be adjusted from the surface to $y_c = -0.1m$. This was achieved by adjusting the supports on both sides of the WEC model, and was estimated to be accurate to $\pm 0.5mm$. In accordance with findings from previous experimental investigations performed in the same facility, the submergence was kept constant in the present study at the optimal value of $|y_c| - R = 15mm$.

3.3 Wave Gauges

Two wire type wave gages for wave height measurements were placed at a distance of $1.17m$ up- and down-stream of the WEC main shaft. The measurement of water level was by electrical resistance measurement. The wave gages were operated with 2.5 V, 5kHz AC and consisted of two stainless steel wires and a ground electrode. The signal from the wave gages was first filtered by a high-pass analog filter to remove any DC offset, then rectified and again low-pass filtered with a corner frequency of 200Hz before it was amplified and digitized by a 10 bit A/D converter. The resulting measurements were transmitted over the same CAN bus system that the main shaft controller employed, using CANOpen as the data protocol. The wave gages were calibrated for a measurement range of $y_m = \pm 50mm$ before each measurement session, and the calibration was repeated after the
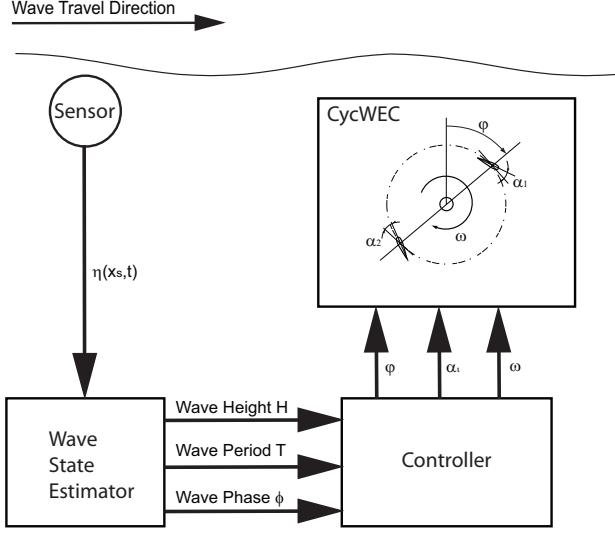
Figure 5. Block diagram of sensing and feedback control approach

last measurement run to verify that no drift in calibration had occurred. The overall accuracy and repeatability of the wave gage measurements was estimated to be better than $\pm 0.1mm$ based on the repeat calibration results, or $\pm 0.5\%$ of the design wave height.

3.4 DAQ and Post Processing

The entire experiment was controlled by a WINDOWS XP PC, using software written in LABView to transmit data over the CAN bus (Controller Area Network) to operate the wave maker, the wave gauges and the CycWEC. The received data was stored in Matlab files for post-processing. The sample rate of the system was 100 Hz for both position control as well as data acquisition, where all transmitted messages where synchronized using the CANOpen sync messages. Every measurement lasted 61 seconds, but only the last 40 seconds when the flow had reached a periodic state were used for data analysis by means of Fourier transform to determine wave heights.

3.5 Feedback Control

A sketch of the overall control and estimation scheme is shown in figure 5. The signal from the up-wave wave gage is used for feedback control, and processed first by the state estimator. The results of the state estimation algorithm are the instantaneous wave height H, wave period T, and wave phase ϕ. These quantities are then used by the controller to prescribe the main shaft angle ϕ as well as the pitch of the blades. The following subsections describe the estimator and controller in more detail.

For the successful cancellation of an unknown, incoming harmonic wave, feedback control and wave state estimation were

necessary. Algorithms to interpret and estimate the wave state in real time fashion were needed to adequately control and efficiently extract energy. The wave state for a single airy wave was defined as phase ϕ, frequency ω, and wave height H. While different types of sensors which measure the water elevation over time may be employed, the wave gage that was placed upstream of the CycWEC was used in this study. This measurement was defined as $\eta(t)$ and displayed a periodic signal with unknown frequency and amplitude and was also corrupted by a small amount of high frequency noise. Given a time history of the upstream measurement a relation was sought such that $[\hat{\omega}(t)\hat{\phi}(t)\hat{H}(t)]^T = f([\eta(t), \eta(t-1), \ldots, \eta(t-n)]) + e(t)$ with minimal estimation error, $e(t)$. A typical Fourier analysis fell short because instantaneous phase information was lost in the decomposition. Other digital signal processing methods needed to be implemented.

Because the upstream wave height measurement contained no negative frequency components, the signal could be expressed as an analytic signal such that

$$\eta(t) = \frac{1}{2\pi} \int_0^\infty \eta(\omega)e^{j\omega t} d\omega \qquad (7)$$

A complex representation of a periodic signal is $e^{j\omega t} = \eta(t) + i\hat{\eta}(t)$. The complex component of the analytic signal, which was unknown at this point, was analogous to the Hilbert transformation, $\mathcal{H}[\bullet]$, of the real component; that is $\hat{\eta}(t) = \mathcal{H}[\eta(t)]$. The Hilbert transformation was a linear filter which produced a phase shift of $\pm\frac{\pi}{2}$ over all frequencies present in the signal, $\eta(t)$. In the time domain the transformation for this linear filter was identically the convolution with $\frac{1}{\pi t}$ which is shown as,

$$\mathcal{H}[\eta(t)] = \frac{1}{\pi t} * \eta(t) = \frac{1}{\pi} \int_{-\infty}^{\infty} \frac{\eta(t-\tau)}{\tau} d\tau. \qquad (8)$$

In the frequency domain the transform of the signal $f = \frac{1}{\pi t}$ is

$$-j sgn(f) = \begin{cases} -j & f > 0 \\ 0 & f = 0 \\ j & f < 0 \end{cases} \qquad (9)$$

The transfer function of this ideal filter did have a magnitude of one and a phase of $\pm\frac{\pi}{2}$ for $\pm\omega$, respectively. Because the Fourier transform was a non-causal transformation (dependent on previous, current and future measurements), an approximation to this transformation was necessary. Typical filters such as finite impulse response (FIR) and infinite impulse response (IIR) filters could be designed to simulate the response of $\frac{1}{\pi t}$. For the purposes of this paper, a three-stage cascading IIR filter was used to estimate the complex component of the Hilbert transformation

7

with minimal (although non-linear) phase delays at the design frequency.

Now that the real and complex components of the analytic signal were known to within some degree of error, the instantaneous amplitude was estimated from the L_2 norm of the signals, i.e. $\hat{H}(t) = \|\eta(t) + \hat{\eta}(t)\|_2$. The instantaneous phase was then computed as the angle between the real and complex estimate as, $\hat{\phi}(t) = \arctan(\frac{\hat{\eta}(t)}{\eta(t)})$, and the instantaneous frequency was calculated by the time derivative of the phase estimate.

As seen in figure 5, the wave state is now fully estimated. The control scheme is very basic for the purposes of this paper. Proportional control is used for the blade pitch, such that $\alpha_i(t) = P_g\hat{H}(t)$. This is a reasonable assumption since the open loop wave generation results shown in Siegel et al. [18] display a very linear relationship between the circulation Γ and wave height H. In order to implement rotary control for the wave energy converter the group velocity C_g needs to be estimated and compensated for as a phase delay. The frequency of the passing wave obtained from the estimator and water properties make this a simple calculation. The time delays are then superimposed to control the rotational velocity of the main shaft in a stepwise fashion, such that $\phi(t) = \Phi(t) + \frac{\eta_\lambda}{C_g} + \theta_f$, where C_g is the group velocity of the wave, and θ_f is the phase compensation of the Hilbert transformation filter.

4 Results

The experiments in this study were conducted in two stages. First, experimental runs were performed where the WEC was exposed to a superposition of two harmonic waves. The first wave was at the design point of the wave energy converter and a moderate amplitude, i.e. a wave period of $T = 0.5s$ and a wave flap maker deflection of $\delta = 1.5°$. The second wave period was varied, which results in a modulated wave that exhibits an amplitude modulation with the frequency difference between both waves. The results from these initial experiments are detailed in the next section. In a second testing campaign, the incoming wave was synthesized from a larger number of harmonic waves whose amplitudes followed a Bretschneider power distribution as outlined in the experimental setup section. Here, the center frequency was again at the design point of the WEC, and the number of harmonic wave components was varied.

4.1 Wave Cancellation of Two Component Waves

In figures 6 and 8 a portion of the time signal, and a Fourier Analysis of it are shown, respectively. The flap wave maker is operated to produce a superposition of two waves, with wave periods $T_1 = 0.5s$ and $T_2 = 0.4s$ which produces an incoming wave that is modulated in amplitude with the frequency difference between both. In order to efficiently cancel this wave, the estimator needs to correctly determine the instantaneous wave height. The
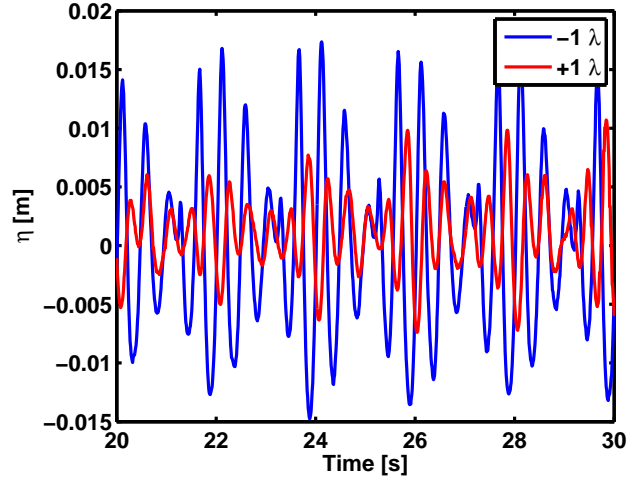

Figure 6. Water surface during feedback controlled wave cancellation of a two component wave system. Incoming wave periods $T_1 = 0.5s$, $T_2 = 0.4s$, wave heights $H_1 = 17mm$ and $H_2 = 10mm$. WEC has two blades, feedback phase $\theta = 197°$, blade pitch gain $G_p = 400°/m$, submergence $|y_c| - R = 15mm$.

estimated wave height at the wave energy converter is shown in figure 8. This estimate is used to change the blade pitch as outlined in the section detailing the feedback control setup. As a result of the wave energy conversion, all wave heights down-wave of the WEC are reduced in amplitude, for the first wave component from $H_{-1} = 16mm$ to $H_1 = 4mm$, and for the second wave component from $H_{-2} = 10mm$ to $H_2 = 5mm$. The efficiency of wave cancellation in this case is 77% accounting for power in all waves.

In figures 9 and 10 a portion of the time signal, and a Fourier Analysis of it are shown, respectively. The flap wave maker is again operated to produce a superposition of two waves, this time with wave periods $T_1 = 0.5s$ and $T_2 = 0.364s$ which produces an incoming wave that is modulated in amplitude with the frequency difference between both that is larger than in the previous case, causing a faster modulation of the wave height. The WEC is able to follow this modulation, resulting in an overall cancellation efficiency of about 80%, which is comparable to the data shown in the previous case. While not shown, different combinations of two harmonic waves were tested and produced similar results in terms of efficiency. This indicates that feedback control of the blade pitch angle is effective in cancelling incoming waves consisting of multiple plain wave components. While not shown, experiments with different combinations of two plain waves all showed results similar to those in presented in this section, with similar overall cancellation efficiencies.
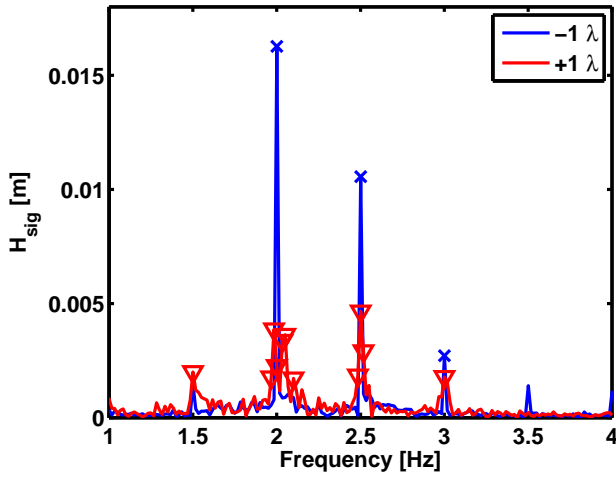
8

Figure 7. Power Spectral Density of the surface elevation at the up-wave and down-wave wave gage. For experimental parameters see caption of figure 6
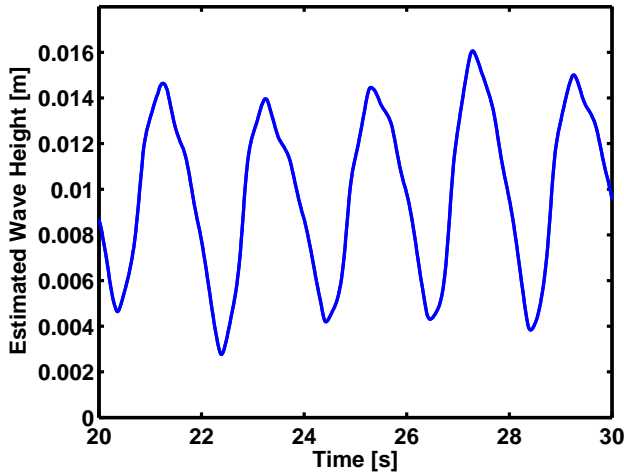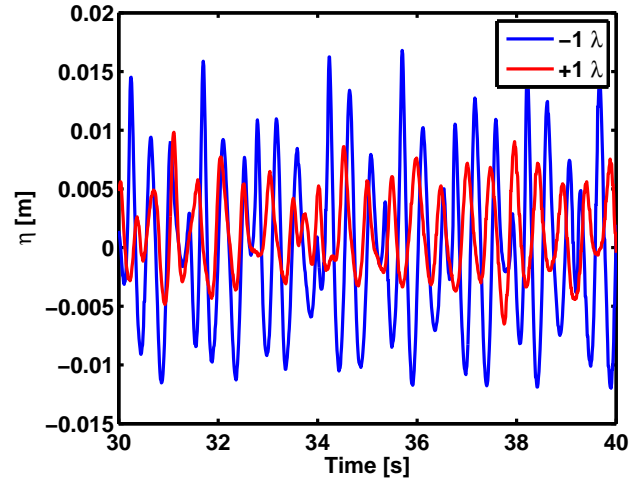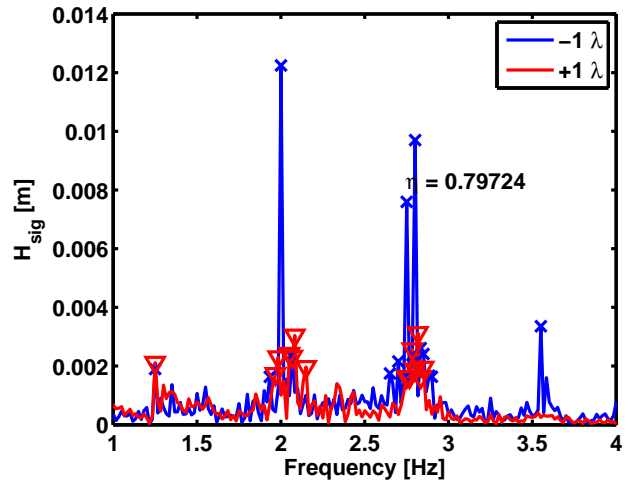

Figure 9. Water surface during feedback controlled wave cancellation of a two component wave system. Incoming wave periods $T_1 = 0.5s$, $T_2 = 0.364s$, wave heights $H_1 = 12mm$ and $H_2 = 10mm$. WEC has two blades, feedback phase $\theta = 197°$, blade pitch gain $G_p = 400°/m$, submergence $|y_c| - R = 15mm$.

Figure 8. Estimated Wave Height at the WEC based on the up-wave gage signal. For experimental parameters see caption of figure 6

Figure 10. Power Spectral Density of the surface elevation at the up-wave and down-wave wave gage. For experimental parameters see caption of figure 9

4.2 Wave Cancellation of Irregular Waves

In this section, first pictures followed by data from typical feedback controlled wave cancellation runs are presented. A side view as well as a view of the experiment from above are shown in figures 11 and 12, respectively. The incoming wave, which is travelling left to right in both pictures, can be observed to be of large wave height up-wave of the CycWEC, and greatly reduced wave height down-wave of the CycWEC.

Wave gage data from a typical feedback controlled experiment run, as observed by the up-wave and down-wave wave

gages, is shown in figure 13. It can be observed that the wave height down-wave is greatly reduced in amplitude, indicating energy extraction by the CycWEC.

Analysis of data acquired after the system had reached a periodic state, i.e. after $t = 20s$, was performed using a Fourier transform. The results for both wave gages are shown in figure 14. The wave components of the incoming wave follow in
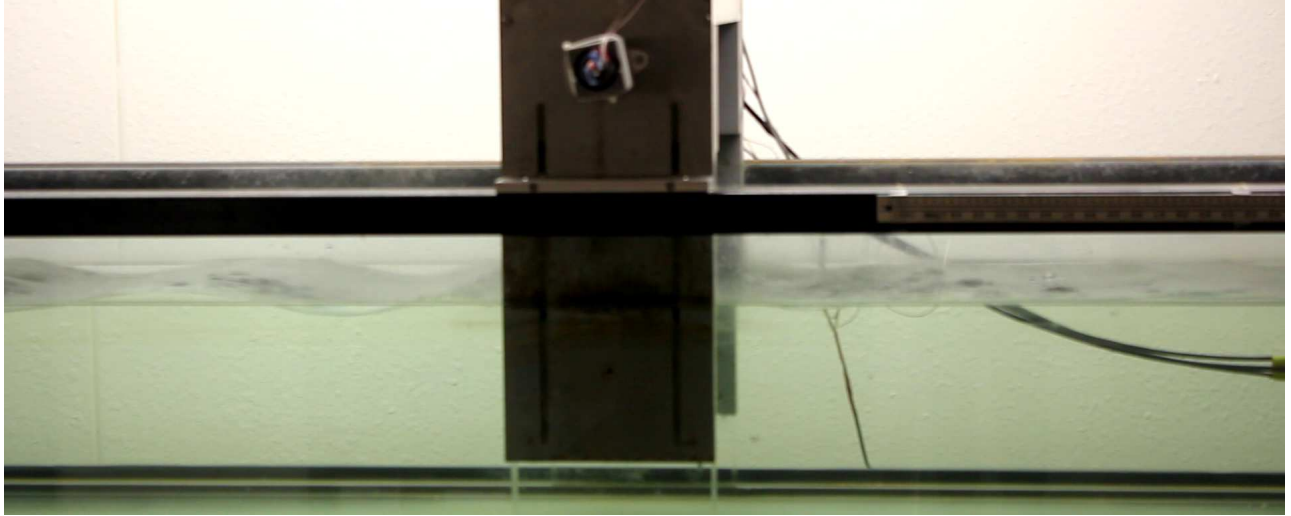
Figure 12. Picture of wave cancellation from side. For experimental parameters see caption figure 11
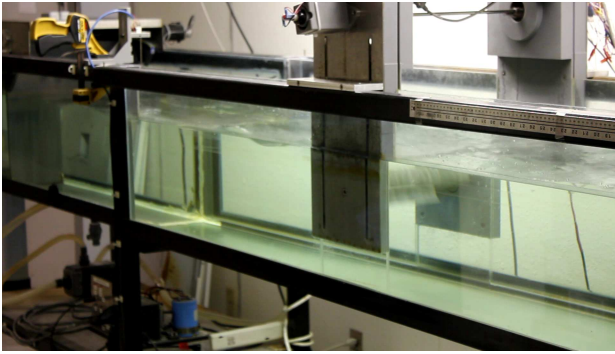

Figure 11. Picture of wave cancellation from down-wave above. Incoming wave follows a Bretschneider spectrum with center period $T = 0.5s$, significant wave height $H_s = 15mm$, and seven individual wave components. WEC has two blades, feedback phase $\theta = 197°$, blade pitch gain $G_p = 400°/m$, submergence $|y_c| - R = 15mm$.

Figure 13. Up-wave and down-wave water surface during feedback controlled wave cancellation. For experimental parameters see caption figure 11

their wave height a Bretschneider distribution, while the down-wave wave heights have been reduced for all wave components. Consequently, an overall inviscid efficiency of 77% was achieved in extracting energy from the incoming wave system.

For comparison to the present experimental results shown in figure 14, numerical simulation results for a 7 component Bretschneider wave are shown in figure 15. These results have been presented earlier in Jeans et al. [11], where the numerical details of the simulation along with other pertinent results can be found. The numerical simulation achieved at 85% a slightly higher overall efficiency for the 7 component Bretschneider wave cancellation. However, both spectra show similar reduction in wave heights for all waves, as can be seen by comparing figures 14 and 15.
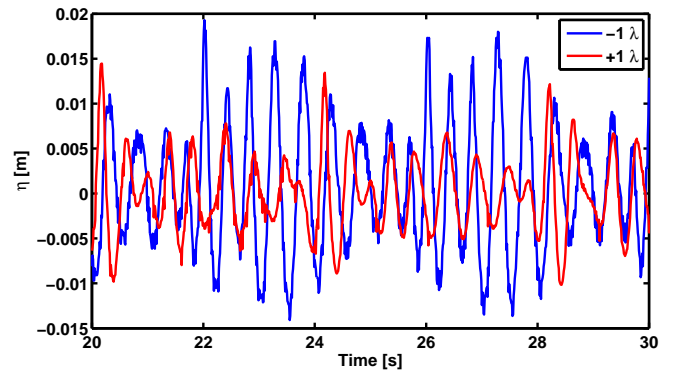
5 Conclusion

Wave cancellation results for a Cycloidal Wave Energy Converter (CycWEC) model in a 1:300 scale wave tunnel experiment are presented. The wave energy converter was operated under feedback control using a wave gage signal as input for a wave estimator and CycWEC controller. The CycWEC was exposed to waves either consisting of two sinusoidal Airy waves, or a larger number of Airy waves following a Bretschneider distribution in wave power. The latter is a good representation of a deep ocean wave field.

Based on the data presented in the preceding section, it is concluded that the CycWEC under feedback control is able to efficiently cancel incoming irregular waves. Inviscid conversion efficiencies around 80% for a range of wave heights and wave periods around the design wave of the CycWEC were demon-
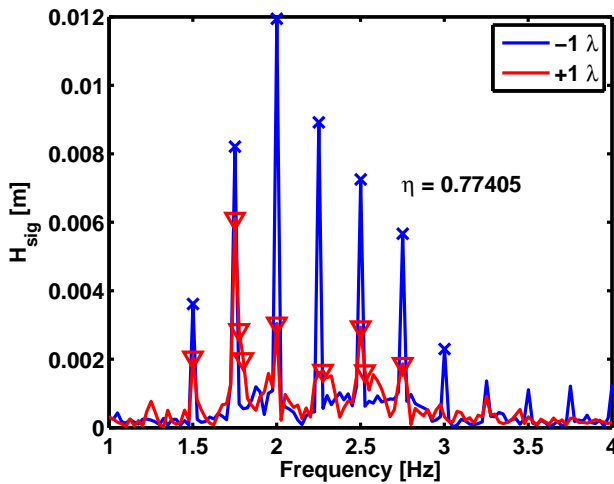
Figure 14. Power Spectral Density of the surface elevation at the up-wave and down-wave wave gage. For experimental parameters see caption of figure 11
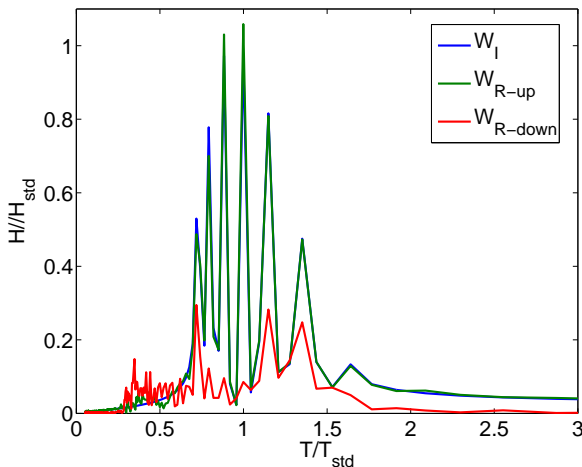

Figure 15. Numerical wave cancellation results from potential flow simulations of a Bretschneider spectrum composed of 7 individual component waves as reported in Jeans et al. [11], numerical details see there. Power Spectral Density of the surface elevation at one standard wave length up-wave and down-wave wave from the WEC.

strated. The efficiency was reduced for wave components where the wave periods were further away from the design wave period. The latter behavior was expected based on earlier simulation results that found reduced efficiency once the ratio between wave celerity and blade travel velocity was changed from unity, see Siegel et al. [3] for details. The overall agreement between the numerical potential flow simulations presented by Jeans et al. [11] and the data presented here was very good, and demon-

strated the capability of the CycWEC to efficiently extract energy from irregular deep ocean waves.

While the current experiment was limited to indirect wave cancellation efficiency measurements due to its small size, experiments are planned at 1:10 scale for Spring of 2012 at the Texas A&M Offshore Technology Research Center. These will allow for direct shaft power measurements and thus overall efficiency measurements accounting for all losses from wave to shaft. Predictions based on published hydrofoil data, however, do allow an estimate for these losses at less than 30% of the incoming wave power; see Siegel et al. [3] for details.

ACKNOWLEDGMENT

REFERENCES

[1] Boyle, G., 2004. *Renewable Energy - Power for a sustainable future*. Oxford University Press.

[2] Bedart, R., 2005. Final summary report - offshore wave power feasibility demonstration project. Tech. rep., E2I EPRI Global, WP 009 - US Rev 1.

[3] Siegel, S. G., Jeans, T., and McLaughlin, T., April 2011. "Deep ocean wave energy conversion using a cycloidal turbine". *Applied Ocean Research,* **Volume 33 Issue 2**, pp. pp. 110–119.

[4] Evans, D. V., 1976. "A theory for wave-power absorption by oscillating bodies". *J. Fluid Mech.,* **77**(1), pp. 1–25.

[5] Betz, A., 1920. "Das maximum der theoretisch möglichen ausnützung des windes durch windmotoren". *Zeitschrift für das gesamte Turbinenwesen,* **26**, p. 307309.

[6] Salter, S. H., 1989. "World progress in wave energy-1988". *International journal of ambient energy,* **10**(1), pp. 3–24.

[7] Evans, D. V., Jeffrey, D. C., Salter, S. H., and Taylor, J. R. M., 1979. "Submerged cylinder wave energy device: theory and experiment". *Applied Ocean Research,* **1**(1), pp. 3–12.

[8] Siegel, S. G., filed in 2006, awarded 2010. "Cyclical wave energy converter". *U. S. Patent 7,686,583 and pending / awarded International Patent applications*.

[9] Hermans, A. J., van Sabben, E., and Pinkster, J., 1990. "A device to extract energy from water waves". *Applied Ocean Research Computational Mechanics Publications,* **Vol. 12, No. 4**, p. 5.

[10] Siegel, S., Roemer, M., Imamura, J., Fagley, C., and Mclaughlin, T., 2011. "Experimental wave generation and cancellation with a cycloidal wave energy converter". In 30th International Conference on Ocean, Offshore and Arctic Engineering (OMAE), no. OMAE2011-49212.

[11] Jeans, T., Siegel, S. G., Fagley, C., and Seidel, J., 2011. "Irregular deep ocean wave energy conversion using a cycloidal wave energy converter". In 9th European Wave and Tidal Energy Conference (EWTEC),Southampton, UK, September 5th 9th.

[12] Siegel, S., Fagley, C., Roemer, M., and McLaughlin, T., 2011. "Experimental wave cancellation using a cycloidal wave energy converter". In 9th European Wave and Tidal Energy Conference (EWTEC),Southampton, UK, September 5th 9th.

[13] Seelig, W., 1983. "Wave reflection from coastal structures". In Proceedings of Coastal Structures, American Society of Civil Engineers (ASCE), pp. 961–973.

[14] Cruz, J., 2008. *Ocean wave energy: current status and future prepectives*. Springer-Verlag.

[15] Newman, J. N., 1977. *Marine Hydrodynamics*. MIT Press.

[16] McTaggart, K., September 2003. Modelling and simulation of seaways in deep water for simulation of ship motions. Tech. Rep. Tech. Rep. DRDC Atlantic TM 2003-190, Defence R&D Canada - Atlantic.

[17] , 1978. "Ittc seakeeping committee report". In 15th International Towing Tank Conference, The Hauge, The Netherlands.

[18] Siegel, S., Seidel, J., and McLaughlin, T., 2009. "Experimental study of aero-optical distortions in a free shear layer". In AIAA Paper 2009-0361.